Application of DIC to Extract Full Field Thermo-Mechanical Data From an HTS Coil

J. Pelegrin, W. O. S. Bailey, and D. A. Crump

***Abstract*—A digital imaging correlation (DIC) test setup was developed to accurately record the contraction of a Bi-2223 superconducting racetrack coil conduction cooled to 154 K. The coil was gripped at both ends to simultaneously measure the load and displacement induced by its own contraction. Postprocessing of the DIC data derived the displacement and strain fields from two areas of interest. The global deformation of the coil structure was influenced by how it was restrained, but the stress-strain curve in the *y*-direction of the HTS coil was established, and its stiffness when under thermally induced strain was found to closely match that of the epoxy resin. The coefficient of thermal expansion determined from the strain-temperature curve was in the same order of magnitude as dilatometer measurements performed upon a sample removed from a similar coil and the difference attributed to small variability in the temperatures across the coil and the mechanical restraint placed on the coil.**

***Index Terms*—HTS coils, stress, strain measurement.**

I. Introduction

THE thermo-mechanical stresses in superconducting coils are usually modelled and rightly focused upon evaluating their impact upon the conductor. Models are normally validated by mechanical tests performed on coupon size specimens removed from sample coils and instrumented with strain gauges [1]–[3]. However, the composite construction and complex shapes of superconducting coils (e.g., racetrack) introduce geometrical inhomogeneities and stress concentrations that often reduce confidence in Finite Element (FE) models of their stress-strain and strain-temperature dependent behaviour.

Non-invasive optical techniques can be applied to measure the global response of the coil, e.g., techniques like Digital Speckle Pattern Interferometry (DSPI) have been applied to study deformations of HTS tapes [4].

DIC is a well-established technique that tracks the displacement of pixelated blocks from a series of digital images to measure surface deformation down to one part per million of the field of view [5]. The full 2-D or 3-D deformation vector fields and strain maps are developed after post processing with software algorithms. The technique is very cost effective and eliminates the subjectiveness of placing/integrating strain gauges that capture only localised strain data. The application of DIC at elevated temperatures has been successful [6]–[8] with many operators opting for non-convective heating methods. The application of DIC at cryogenic temperatures is almost untried [9] and presents new challenges, to assess the robustness of speckle patterning and to develop an appropriate cooling technique.

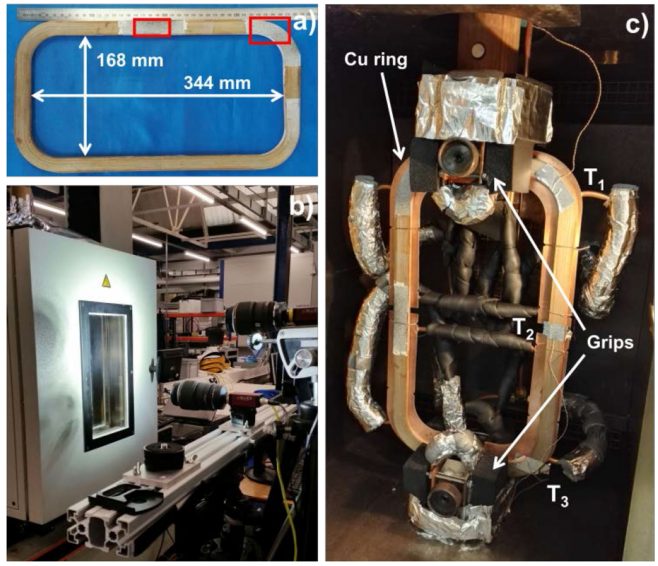

Fig. 1. (a) Superconducting coil (red boxes mark the locations where images were taken), (b) environmental chamber and camera setup (c) coil gripped in the machine jaws with cooling pipework and thermalising Cu ring shown. T-type thermocouples T_1, T_2, T_3 are located at the top, middle and bottom of the coil respectively.

II. Experimental Setup and Tests

A. Coil Description

The HTS coil under assessment is shown in Fig. 1(a). It consists of 40 turns of Ag sheathed high strength reinforced Bi-2223 tapes interleaved by a fiberglass sheet and potted with Stycast 1622. The coils long and short inner diameters are 344 mm and 168 mm respectively. Its width = 19.3 mm, thickness = 7.5 mm and corner bend radius = 39 mm [10].

B. DIC Setup

The experimental setup is shown in Fig. 1(b). The tests were performed inside an Instron 4204 test machine fitted with an environmental chamber. The 400 mm × 200 mm viewing window consisted of two panes of heated glass separated by a void

Manuscript received September 19, 2017; accepted February 11, 2018. Date of publication February 19, 2018; date of current version May 4, 2018. *(Corresponding author: J. Pelegrin.)*

The authors are with the University of Southampton, Southampton SO17 1BJ, U.K. (e-mail: jpm1c13@soton.ac.uk; wosb@soton.ac.uk; dac400@soton.ac.uk).

Color versions of one or more of the figures in this paper are available online at http://ieeexplore.ieee.org.

Digital Object Identifier 10.1109/TASC.2018.2807376

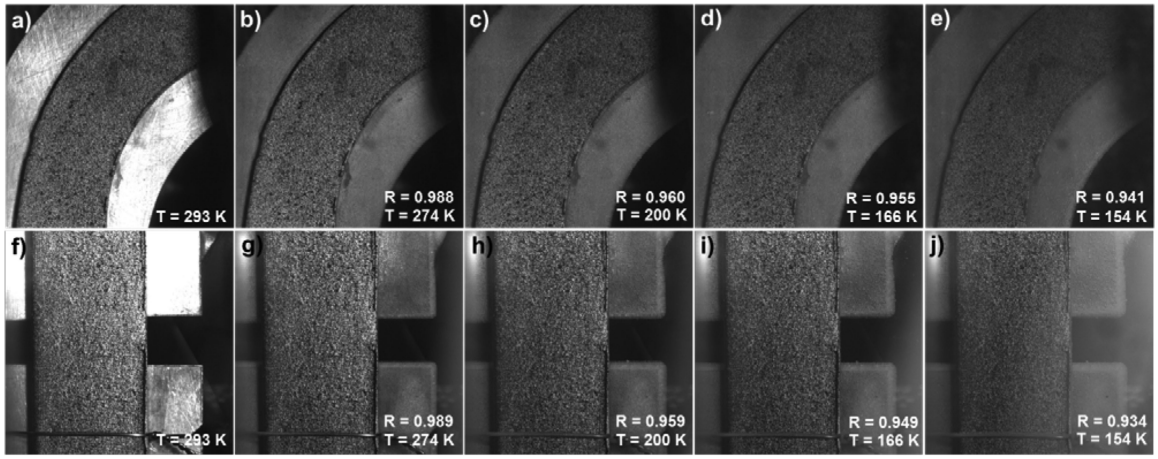

Fig. 2. Images of the (a)–(e) top corner and (f)–(j) middle section of the coil taken at different temperatures during the cooling down. The correlation factor has been included to indicate the degradation of the image quality during the process.

space of air. The images were captured using two Manta MG 504B ASG cameras from Allied Vision Technologies fitted with Sigma 105 mm F/2.8 EX DG Macro lenses. Two Nila Zaila lights were used for illumination.

Prerequisite work performed upon glass fiber coupons convection cooled to refrigeration temperatures (253 K) in the same chamber identified a number of problems with the setup that influenced the quality of the DIC correlation. The chamber is not vacuum tight and condensation tended to form on the inside of the optical window, particularly in the regions where the sample was illuminated from. Vapor ripples travelling across the surface of the sample, caused by the natural convection loops circulating inside the chamber during cooling, increased the deviation (noise) in the strain measurement from ± 0.0002 mm/mm to ± 0.01 mm/mm. Similar effects are discussed in [11] for DIC tests at elevated temperatures.

Consequently, some adaptations were made to the cooling technique. The coil was placed inside the environmental chamber (purged with dry nitrogen) and clamped in the grips. The chamber's force flow gas cooling system and window heaters were disabled in favor of locally cooling the coil by conduction with liquid nitrogen (LN_2). A heat exchanger fed with LN_2 was coupled to each grip and a split copper ring positioned behind the coil to improve the distribution of cooling as in Fig. 1(c). Copper wire ties were used to bring the coil and copper ring in better contact, however, the coil was still able to slide freely against the rings, except in the gripped region. A positive pressure was maintained inside the chamber by recirculating the cold return gas in at the top (behind the coil) with the chamber fan operating, and venting gas from the bottom of the chamber.

A separate digital camera focusing on each speckled region was synchronized with a StarTech acquisition controller card and LabVIEW software to take an image and record the load measured by the Instron's load cell every minute during cool down. The local temperature of the coil was recorded with thermocouples connected to an Agilent 34970A data logger.

C. Speckle Pattern

Prior to installation of the coil in the chamber, a speckle pattern was applied to the coil by masking off two regions and spraying a solid layer of matt white paint, followed by a fine spray of black paint to produce small randomly distributed speckles. A good pattern should have a broad contrast between black and white to enhance detection of intermediate greyscale values and the uniqueness of each signature is only guaranteed if the surface has a non-repetitive and isotropic pattern. The corner of the coil in Fig. 2(a)–(e) and straight section in Fig. 2(f)–(j) both have an area of interest (shown in Fig. 1(a)) of $\sim$45 mm $\times$ 19 mm and the full width of the coil is included in the field of view to use the edges of the coil as a reference point to confirm its free movement against the copper ring.

D. Test Execution

The sequence of camera images presented in Fig. 2 represent five pairs of images taken at 0, 20, 40, 60 and 75 minutes during cool down. The corresponding temperature recorded at the middle of coil is included in each image. Differences in the temperature gradients measured between the top-to-middle ($\Delta T_{12} = 4$–5 K) and middle-to-bottom ($\Delta T_{23} = 8$–10 K) sections of the coil were caused by heating from the external lights. After 20 minutes, a reduction in luminosity is evident, and the shiny surface of the Cu ring behind the coil darkens as ice begins to form. Thereafter, the illumination in each image remains constant despite condensation forming on the inside of the window, caused from heating by the external lights. The cameras field of view was fortunately unaffected by the patches of condensation. Images (e) and (j) show a "mist" of vapour approaching from the right represented by "blurring" in the images. The test was subsequently stopped after 75 minutes.

E. Post-Processing

A DIC software package (MatchID) was used to process the 2-D displacements and strains from the array of images. The software interrogates two images at different states of displacement. They are compared by using a pixel and its signature in the undisplaced image, and searching for the same pixel in the displaced image to satisfy a given similarity function. This function is usually based on a least-squares formulation.

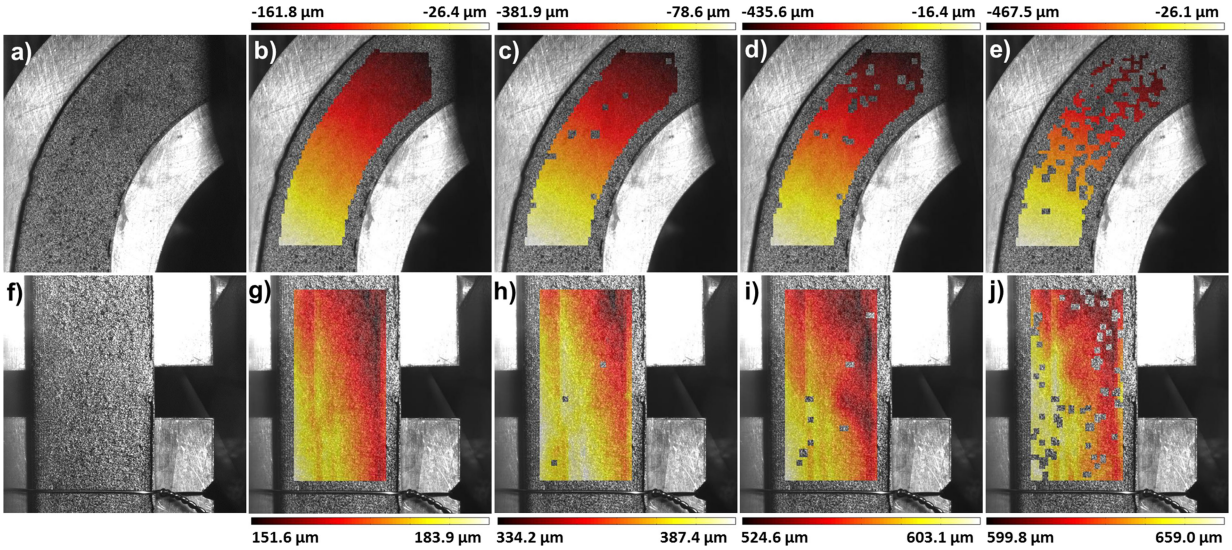

Fig. 3. Horizontal displacements produced on the (a)–(e) top corner and (f)–(j) middle section of the coil obtained in the DIC analysis. Temperatures at which these were images were captured match the corresponding labelled images in Fig. 2.

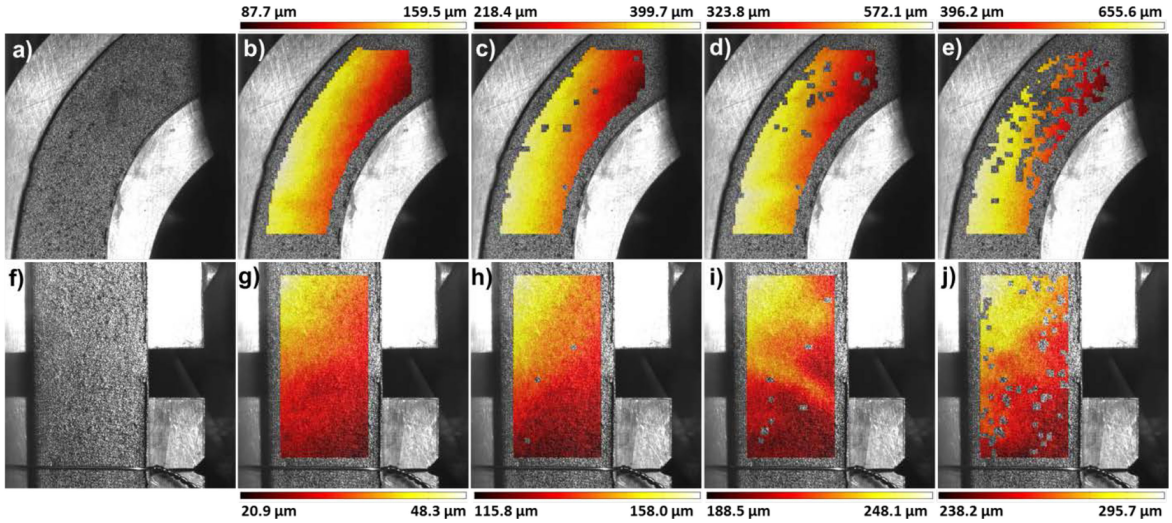

Fig. 4. Vertical displacements produced on the (a)–(e) top corner and (f)–(j) middle section of the coil obtained in the DIC analysis. Temperature at which these were images were captured match the corresponding labelled images in Fig. 2.

A subset size (collection of pixels) and step size (number of pixels over which the subset is shifted in the x- and y-direction to calculate the next result) must be defined as inputs. The size of a subset can be, e.g., 7×7, 11×11, 15×15 pixels, etc. and should contain at least three unique features. The step size can be 3, 5, 7 pixels, etc. and often sized so subsets overlap.

Using guidelines from [12], a square subset of 51 pixels and step size of 25 pixels were applied. Therefore, one pixel equates to 16 μm, giving a total measurable displacement of 1.26 mm.

The correlation factor, R, output by the software (embedded in the bottom right corner) in Fig. 2(a)–(j) gives an indication of the effectiveness and accuracy of the Zero Normalized Sum Square Difference (ZNSSD) correlation performed between "displaced" images and the reference image. An $R > 0.8$ is generally regarded as reliable [12] and therefore, the R values in Fig. $2 > 0.9$ suggest very good accuracy.

III. Results

A. Coil Displacements

The color contours in Fig. 3(a)–(j) show how the coil contracts in the horizontal (x-direction) at the five temperature conditions; 293, 274, 200, 166, and 154 K. The corner of the coil in Fig. 3(a)–(e) extends outwards with reducing temperature. The distribution of displacements is lowest near the region where coil is gripped and follows the curvature of the tapes. The greatest extension of 475 μm (659 μm$-$184 μm) occurs at the straight part of the coil as it begins to straighten. This equates to $\sim$0.8% of the racetracks short radius dimension (93.5 mm to the middle of coil) in the x-direction. In contrast, the outer edge of the corner of the coil displaces negatively in Fig. 3(a)–(e) and bows outwards from the centre of the racetrack.

The greatest displacement (-305 μm ($\sim -0.3\%$)) is found on the inner edge of the corner section on approach to the grips.

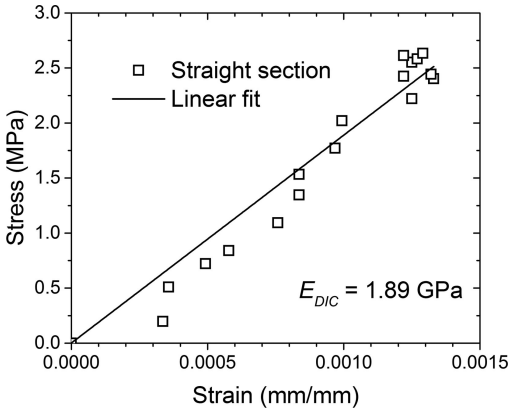

Fig. 5. Stress-strain data points (□) obtained from the DIC analysis with the linear fit (solid line) used to evaluate E_{DIC}.

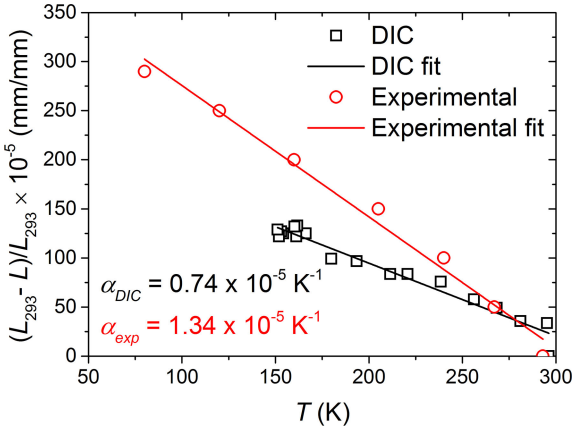

Fig. 6. Linear coefficient of thermal expansion plotted as function of temperature obtained from the DIC analysis (□) and experimental measurements. The corresponding solid lines are used to evaluate α_{DIC} and α_{exp} respectively.

Some inconsistent behavior is observed near the copper tie in Fig. 3(f)–(j). This region begins contracts inwards and relaxes after 166 K. It seems the copper tie, needed to improve the contact between the rear of the coil and the Cu ring, actually influenced the movement of the straight section in the *x*-direction, despite it being free to slide at ambient.

The color contours in Fig. 4(a)–(j) show how the vertical (*y*-direction) displacements evolve when reducing temperature. From Fig. 4(a)–(e), the total difference in free displacement in the corner of the coil (measured from start to end of test) between the regions of maximum displacement 496 μm (655.6 μm−159.5 μm) and minimum displacement 309 μm (396.2 μm−87.7 μm) is 187 μm.

The vertical displacements are mapped in Fig. 4(f)–(j) for the straight section of the coil. The maximum displacement of 248 μm (295.7 μm−48.3 μm) occurs on the outer edge of coil approaching the corner. This equates to ∼0.13% of the racetracks long radius dimension (181.5 mm to middle of coil) in the *y*-direction, and is 6 times lower than the corresponding extension in the *x*-direction of coil. These results clearly demonstrate the gripping has impaired the coils natural contraction in the *y*-direction. The patchy contour plots in images (e) and (j) of Figs. 3 and 4 highlight the deterioration of the DIC correlation due to the vapor mist and condensation.

B. Stress-Strain Curve

The strain at the surface of the coil can be derived from the same collection of images and using the "virtual strain gauge" feature in MatchID. The size of this virtual strain gauge was defined as 5.8 mm, which is relatively large (∼1/3 width of the coil) to improve strain resolution, given no sudden changes in strain were expected [12]. The strain derived by the software in the vertical *y*-direction, from all the measured points during the cool down, is plotted against the corresponding force (N) translated to stress (MPa) in Fig. 5. The slope of the stress-strain curve produces a stiffness $E_{\mathrm{DIC}} \approx 1.9$ GPa during the cooling down. This stiffness corresponds well with the elastic modulus of Stycast 1266 epoxy resin at low temperatures, which varies between 1.3–2.5 GPa between 293 K and 150 K [13]. The linear coefficient of thermal expansion (CTE) of Stycast 1266 at low temperature ($\alpha_{\mathrm{exp}} = 3.7 \times 10^{-5}$ K^{-1}) [14] is ∼3.5 times greater than G10 fibreglass and ∼2 times greater than the conductor constituents [15]. It suggests the resin is the most reactive component in the composite coil structure at low temperatures and low strains.

C. Strain-Temperature Curve

The thermally induced strain in the straight section of coil in the *y*-direction derived by DIC is plotted against temperature (□) in Fig. 6. This curve is plotted together with an experimental measurement of a sample removed from a similar coil using a cryogenic dilatometer setup (○) [16]. The slopes of the curves represent the linear CTE of the composite coil and are $\alpha_{\mathrm{DIC}} = 0.74 \times 10^{-5}$ K^{-1} and $\alpha_{\mathrm{exp}} = 1.34 \times 10^{-5}$ K^{-1} respectively. The CTE value obtained by DIC is ∼2 times smaller than measured with the dilatometer. This difference may be accounted for by gripping imposed *at both ends* of the coil and small temperature gradients measured across the length (*y*-direction) of the coil during cooling.

IV. Conclusion

This novel piece of work has confirmed that DIC can be successfully deployed at cryogenic temperatures. The speckle pattern can survive at these extreme temperatures and provide high fidelity full field data. The displacements and strains that occur in complex components like HTS racetrack coils were mapped over larger regions to reveal complex interactions that would probably be missed if applying strain gauges.

The stress-strain and strain-temperature curves were produced to derive a coil stiffness (in the *y*-direction) induced by reducing temperature that matched well with the stiffness of the resin, and a linear CTE partly influenced by the configuration used to grip the coil and measure the force of contraction. The remaining challenges to improve the existing setup include, building and conducting further tests in a bespoke vacuum chamber and uniformly supporting and compressing the coil to match the configurations typically deployed in HTS machines.

REFERENCES

[1] C. Barth, G. Mondonico, and C. Senatore, "Electro- mechanical properties of REBCO coated conductors from various industrial manufacturers at 77 K, self-field and 4.2, 19T," *Supercond. Sci. Technol.*, vol. 28, Art. no. 045011, Feb. 2015

[2] C. Minas and L. Salasoo, "Three-dimensional thermal stress in a superconducting coil assembly," *IEEE Trans. Mag.*, vol. 27, no. 2, pp. 2381–2383, Mar. 1991.

[3] S. Choi, T. Kiyoshi, S. Hahn, and M. Sugano, "Stress analysis of a high temperature superconductor coil wound with Bi-2223/Ag tapes for high field HTS/LTS NMR magnet application," *IEEE Trans. Appl. Supercond.*, vol. 19, no. 3, pp. 2237–2240, Jun. 2009.

[4] L. A. Angurel *et al.*, "Quench detection in $YBa_2Cu_3O_{7-\delta}$ coated conductors using interferometric techniques," *J. Appl. Phys.*, vol. 104, Nov. 2008, Art. no. 093916.

[5] A. E. Bartali, V. Aubin, and S. Degallaix, "Fatigue damage analysis in a duplex stainless steel by digital image correlation technique," *Fatigue Fract. Eng. Mater Struct.*, vol. 31, no. 2, p. 137–151, Feb. 2008.

[6] S. Zhang, J. M. Dulieu-Barton, R. K. Fruehmann, and O. T. Thomsen, "A methodology for obtaining material properties of polymeric foam at elevated temperatures," *Exp. Mech.*, vol. 52, pp. 3–15, 2012.

[7] J. L. Walley, R. Wheeler, M. D. Uchic, and M. J. Mills, "In-situ mechanical testing characterizing strain localization during deformation at elevated temperatures," *Exp. Mech.*, vol. 52, pp. 405–416, 2012.

[8] C. M. Casperson, J. D. Carroll, J. Lambros, H. Sehitoglu, and R. H. Dodds, "Investigation of thermal effects on fatigue crack closure using digital imaging correlation experiments," *Int. J. Fatigue*, vol. 61, pp. 10–20, 2014.

[9] O. Hatamleh, R. S. Mishra, and O. Oliveras, "Peening effects on mechanical properties in friction stir welded AA 2195 at elevated and cryogenic temperatures," *Mats. Design*, vol. 30, pp. 3165–3173, 2009.

[10] B. Xu, "Design, construction, and test of a 100 kVA high temperature superconducting demonstration synchronous generator," Ph.D. dissertation., Inst. Cryogen., Univ. Southampton, Southampton, U.K., Sep. 2008.

[11] J. Min, L. G. Hector, L. Zhang, L. Sun, J. E. Carsley, and J. Lin, "Plastic instability at elevated temperatures in a TRIP-assisted steel," *Mats. Design*, vol. 95, pp. 370–386, 2016.

[12] P. Lava, "Practical considerations in DIC measurements" in *Proc. 10th Int. Conf. Adv. Exp. Mech.*, Edinburgh, U.K., Sep. 2015. [Online]. Available: http://www.matchidmbc.be/Presentation/Edinburgh_DIC_2015.pdf

[13] T. Hashimoto and A. Ikushima, "Mechanical properties of Stycast-1266 at low temperatures" *Rev. Sci. Instrum.*, vol. 51, Mar. 1980, Art. no. 378.

[14] G. W. Swift and R. E. Packard, "Thermal contraction of Vespel SP-22 and Stycast 1266 from 300 K to 4 K," *Cryogenics*, vol. 19, pp. 362–363, Jun. 1979.

[15] S. W. Van Sciver, "Helium cryogenics," in *International Cryogenics Monograph Series*, New York, NY, USA: Springer, 2012.

[16] B. Xu, M. K. Al-Mosawi, Y. Yang, and C. Beduz, "Fabrication and characterization of Bi-2223 coils for generator applications," in *Proc. Int. Cryo. Eng. Conf.*, 2006, pp. 709–712.